Studies of Mechanical Vibrations and Current Harmonics in Induction Motors Using Finite Element Method

P.PAO-LA-OR[*†], S.SUJITJORN[*], T.KULWORAWANICHPONG[*], and S.PEAIYOUNG[**]

[*]School of Electrical Engineering, Institute of Engineering,
Suranaree University of Technology, Nakhon Ratchasima, 30000, THAILAND
[**]RTAF Academy, Air Education and Training Command,
Bangkok, 10220, THAILAND
[†]corresponding author: padej@sut.ac.th

Abstract: - This paper illustrates a numerical approach to magnetic field modeling for a squirrel-cage induction motor fed by various voltage sources: i) an ideal sinusoidal source, ii) a PWM voltage- source-inverter (VSI), and iii) a six-step VSI. A two-dimensional nonlinear time-stepping finite element method (FEM) is used for electromagnetic field approximation when the motor is under a full-load steady-state revolution. To solve this time-dependent problem, the numerical backward-difference integration is applied. Due to the saturation characteristic of the magnetic materials, the combined Newton-Raphson (N-R) with bi-conjugate gradient (BCG) method is employed to handle the nonlinearity and to solve the linearized equations. The approach has been applied to evaluate the mechanical vibrations of the motors in associate with the geometry of the rotor slots. Also, the effects of nonsinusoidal supply voltages on the current harmonics have been investigated.

Key-Words: - Mechanical Vibration, Electromagnetic Force, Computer Simulation, Finite Element Method, Induction Motors, Current Harmonics, Rotor Slots

Notation List:

A	magnetic vector potential
B	magnetic flux density
F	magnetic force
H	magnetic field intensity
$\mathbf{J_0}$	current density
s	slip
t	time
x	x-axis of cartesian coordinate
y	y-axis of cartesian coordinate
∇	curl operator
Δ_e	area of the triangular element
Δt	time interval
$\Delta\theta$	change of rotor position
σ	conductivity
ν	reluctivity

1 Introduction

To design an induction motor requires an accurate prediction of some physical quantities, e.g. magnetic flux density, magnetic force, rotor movement under load or no-load conditions, etc. The main contributor to the motor behaviours is magnetic flux distribution passing through the motor cross-sectional area. In order to understand the motor dynamic, the magnetic flux distribution and the corresponding magnetic force must be known from solving the magneto-dynamic equations of the motor. The works during 1990-1993 [1,2] considered vibrations caused by rotor eccentricity, and supply harmonics produced by inverter sources. The works [3,4] studied the effects of rotor slot skewness on motor vibrations. From 1997 till present, the number of stator and rotor slots has been carefully designed to reduce motor vibrations [5,6]. The study of the shapes of rotor slots that influence the vibrations has not been considered before. This is an important issue addressed by this paper. By our approach, comparison studies of the rotor slot shapes affecting the motor lateral vibrations in associate with three IEEE standard slots [7] have been accomplished. Our studies also considered the effects of nonsinusoidal voltage sources: i) an ideal sinusoidal source, ii) a PWM voltage-source-inverter (VSI), and iii) a six-step VSI.

Two methods commonly used for magnetic flux calculation are permeance wave theory, and numerical approximation methods (e.g. finite difference: FD, finite element methods: FEM, etc) [8]. The disadvantage of the wave approach is its lack of accuracy especially when nonlinearity of magnetic cores is involved. The FD and FEM are applicable to a broad range of solving electromagnetic problems due to their flexibility,

and accuracy. Application of the FEM to analyze the magneto-dynamic of an induction motor is inclusive. This kind of problems is normally represented by nonlinear partial differential equations then discretised into nonlinear FEM equations. The well-known Newton-Raphson (N-R) method is often employed to solve the FEM equations due to its good convergence. The computing can be slow if the simple time-stepping technique is used, albeit. This paper thus addresses the combined N-R and bi-conjugate gradient method (NR-BCG method) to speed up the computing. The computed magnetic forces are used as the external forces causing the lateral vibration. The effects of the rotor slot shapes on vibration are investigated.

In this paper, the mathematical modeling of induction motors for computing purposes with computational and experimental results are presented in Section 2. This includes the magnetic field modeling by FEM, the NR-BCG method, and the FEM-based vibration modeling. Section 3 describes the effects of supply waveforms on current harmonics. Section 4 presents the effects of the rotor-slot geometry on mechanical vibrations and discussions. Conclusions follow in Section 5.

2 FEM for Electromagnetics and Mechanics

2.1 Models and Computational Approach

In magnetic field calculations, the magnetic vector potential **A** carries a bundle of information consisting of field intensity **H**, flux density **B**, and induced magnetic forces **F** [9]. For convenience, some assumptions are made as follows: the magnetic field presents in the cross-sectional (*x,y*) plane, the induced current appears as *z*-component, the magnetic materials of the cores are nonlinearly isotropic, and the displacement currents are negligible due to low supply frequency (50 Hz) [10]. Hence, Eq. (1) describes the temporal and spatial variations of **A** [11], [12]

$$\frac{\partial}{\partial x}\left(\nu\frac{\partial \mathbf{A}}{\partial x}\right)+\frac{\partial}{\partial y}\left(\nu\frac{\partial \mathbf{A}}{\partial y}\right)-s\sigma\left(\frac{\partial \mathbf{A}}{\partial t}\right)+\mathbf{J}_0=0 \qquad (1)$$

, where ν is the reluctivity of the material, σ is the conductivity of the rotor conducting media, s is the motor slip, and $\mathbf{J}_0$ is the applied current density.

With today's computing platforms, solution findings for Eq. (1) employ various numerical methods [13]. Our work has utilized the finite element method (FEM) for solving the equation. Fig. 1 shows the studied semi-closed rotor slot shapes as round trapezoidal, rectangular and round shapes which have equal cross-sectional areas. The cross-section of a motor is discretized into minute triangular elements. Fig. 2 shows one quarter of the discretized cross-section according to the round trapezoidal slot. The entire cross-section of a motor for each slot shape contains 5,224 elements and 2,688 nodes. Among them, meshes are grouped into two, one for the stator and the other for the rotor. The air gap is considered to be two layers, one designated to the stator and the other to the rotor. These meshes are generated once at the beginning of the computing process. During the computing processes, the meshes rotate in accordance with rotor's revolution.

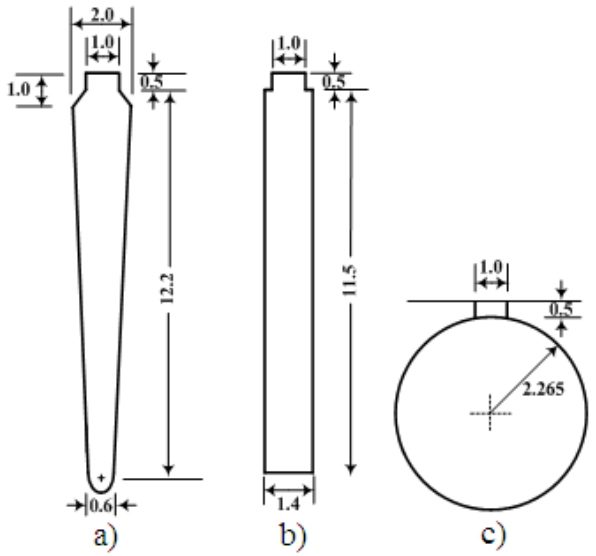

Fig. 1. Dimensions (in mm) of rotor-slot shapes: a) round trapezoidal, b) rectangular, c) round

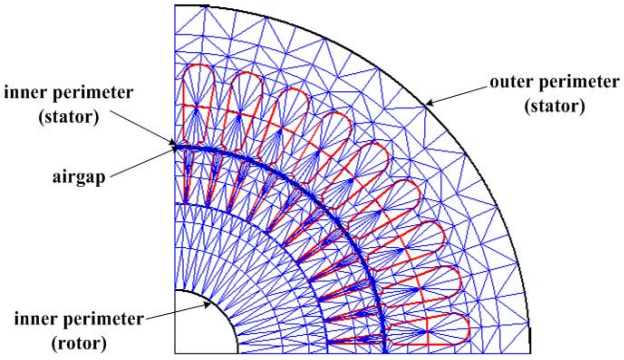

Fig. 2. Discretized cross-section of an induction motor

We adopted the Galerkin weighted residual method [14] to derive the element equation on the basis of the Maxwell's equations. Resulting from Eq. (1) with the Galerkin weighted residual method applied, we arrive at the following expression

$$[M]\{\dot{A}\}+[K]\{A\}=\{F\} \tag{2}$$

, where

$$[M]=\frac{s\sigma\Delta_e}{12}\begin{bmatrix}2&1&1\\1&2&1\\1&1&2\end{bmatrix}$$

$$[K]=\frac{v}{4\Delta_e}\begin{bmatrix}b_ib_i+c_ic_i & b_ib_j+c_ic_j & b_ib_k+c_ic_k\\ & b_jb_j+c_jc_j & b_jb_k+c_jc_k\\ Sym & & b_kb_k+c_kc_k\end{bmatrix}$$

$$\{F\}=\frac{J_0\Delta_e}{3}\begin{bmatrix}1\\1\\1\end{bmatrix}$$

, where Δ_e is the area of the triangular element, which is

$$\Delta_e=\frac{1}{2}\begin{vmatrix}1&x_i&y_i\\1&x_j&y_j\\1&x_k&y_k\end{vmatrix}$$

$$a_i=x_jy_k-x_ky_j,\quad b_i=y_j-y_k,\quad c_i=x_k-x_j$$
$$a_j=x_ky_i-x_iy_k,\quad b_j=y_k-y_i,\quad c_j=x_i-x_k$$
$$a_k=x_iy_j-x_jy_i,\quad b_k=y_i-y_j,\quad c_k=x_j-x_i$$

Eq. (2) describes the magnetic vector potential as a space-time function.

To simulate the motor movement, we need to discretize Eq. (2). We use the backward difference method for the discretization because of its good convergent property [15]. Hence, the time derivatives of the magnetic vector potential can be expressed by

$$\{\dot{A}\}^{t+\Delta t}=\frac{\{A\}^{t+\Delta t}-\{A\}^{t}}{\Delta t} \tag{3}$$

The discrete form of Eq. (2) at time $t+\Delta t$ is

$$[M]\{\dot{A}\}^{t+\Delta t}+[K]\{A\}^{t+\Delta t}=\{F\}^{t+\Delta t} \tag{4}$$

Inserting Eq. (3) into Eq. (4), one could obtain

$$\left(\frac{1}{\Delta t}[M]+[K]\right)\{A\}^{t+\Delta t}=\frac{1}{\Delta t}[M]\{A\}^{t}+\{F\}^{t+\Delta t} \tag{5}$$

To solve Eq. (5) requires an efficient iterative method of solving nonlinear time-stepping equations. We apply the N-R method to solve the equations. Additionally, our approach employs the BCG method as its internal structure to solve linearized equations. The flow diagram in Fig. 3 represents our solution finding process. Regarding to the approach, the matrix form of the N-R equation governing the element can be found as Eq. (6), where the left-most matrix is Jacobian

$$\begin{bmatrix}\frac{\partial G}{\partial A_i^{t+\Delta t}} & \frac{\partial G}{\partial A_j^{t+\Delta t}} & \frac{\partial G}{\partial A_k^{t+\Delta t}}\\ \frac{\partial H}{\partial A_i^{t+\Delta t}} & \frac{\partial H}{\partial A_j^{t+\Delta t}} & \frac{\partial H}{\partial A_k^{t+\Delta t}}\\ \frac{\partial I}{\partial A_i^{t+\Delta t}} & \frac{\partial I}{\partial A_j^{t+\Delta t}} & \frac{\partial I}{\partial A_k^{t+\Delta t}}\end{bmatrix}\begin{bmatrix}\Delta A_i^{t+\Delta t}\\ \Delta A_j^{t+\Delta t}\\ \Delta A_k^{t+\Delta t}\end{bmatrix}=-\begin{bmatrix}G\\H\\I\end{bmatrix} \tag{6}$$

, in which G, H and I represent the first, second and third row equations embedded in Eq. (5), respectively.

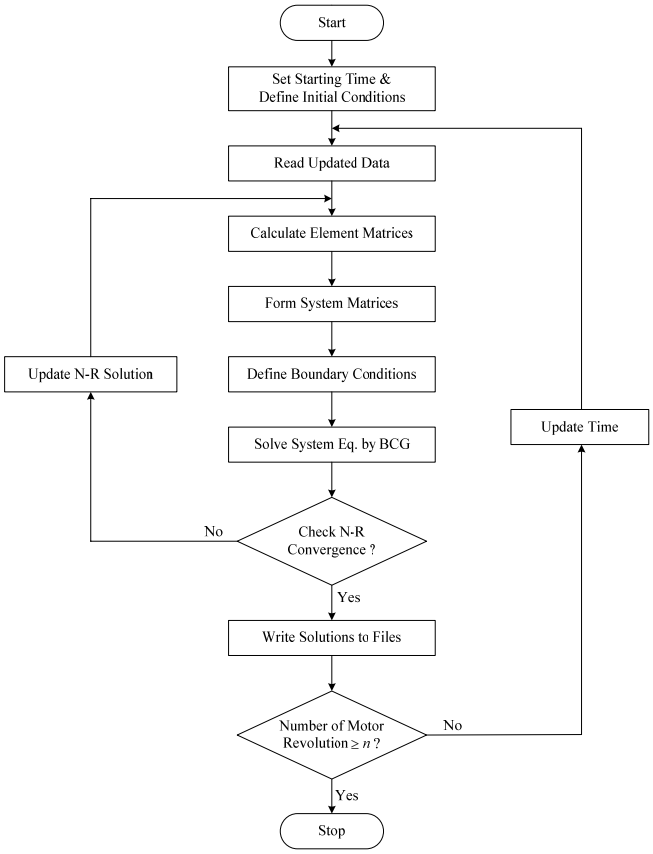

Fig. 3. Flow diagram of the electromagnetic computation

The boundary conditions applied here are zero magnetic vector potentials at the outer perimeter of the stator core, and the inner perimeter of the rotor core as shown in Fig. 2. To speed up the computation, we have used the banded diagonal matrix storage [16] together with the BCG method. In the time-stepping FEM, the information from the last time update can be successfully used as the initial solution to reduce the computing time when solving the FEM equations. The size of each time step, Δt, is fixed at 0.1145 ms which is the time needed for the rotor to turn $\Delta\theta = 1°$ steadily (steady-state operation is assumed). The machine used in this study is a three-phase, four-pole, Y-connected, 5-hp squirrel cage induction motor with a double layer winding of 7/9 pitch coil. The motor possesses 36 stator slots and 44 un-skewed rotor slots. The sinusoidal source provides a 380-V, 50-Hz sinusoidal voltage at full load (slip, s =0.03).

The computation of flux and magnetic forces was conducted using an FEM solver developed in C. Fig. 4 illustrates the flux line distributions through the motor cross-sections corresponding to the round trapezoidal rotor-slot.

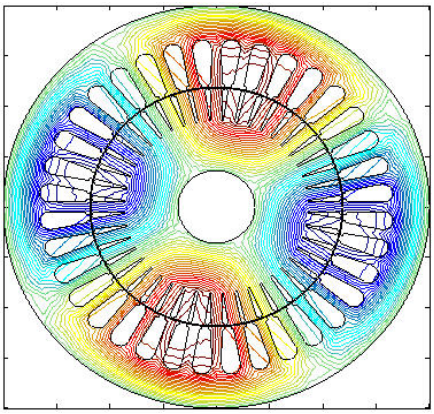

Fig. 4. Flux line distribution (round trapezoidal rotor-slot)

The finite element approach is also utilized to calculate the motor's vibration. The motion can be described by Eq. (7), in which [*M*], [*C*], and [*K*] are the mass, damping, and stiffness matrices, respectively. {*F*} represents the external force vector. As shown in Fig. 5 for our computing of the lateral vibration, the stator core and the motor frame are considered. The corresponding cross section contains 1,343 nodes, and 1,822 elements. It is assumed that the force acting on the center of each stator tooth could be transmitted through to the motor frame [17].

$$[M]\{\ddot{d}\}+[C]\{\dot{d}\}+[K]\{d\}=\{F\} \quad (7)$$

The force applied to the motor is the computed magnetic force at the center of each stator tooth. In addition, the motors are considered to have thin-plate cross sections [18].

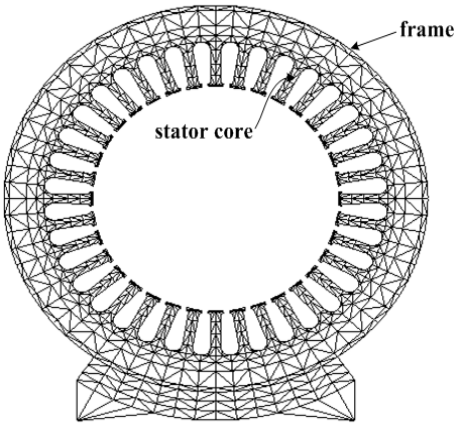

Fig. 5. Triangular elements for computational vibration

Our FEM solver developed in C has been used to solve the motion equation to obtain the lateral vibration solutions. The FEM solver provides solutions disclosing the distortions of the stator inner perimeter as shown in Fig. 6. The solid lines in these figures represent the perimeter in an undistorted situation. The dashed lines show the instantaneous displacement or distortion magnified by 10^9 times. The average displacement in one revolution is 6.0924×10^{-8} mm.

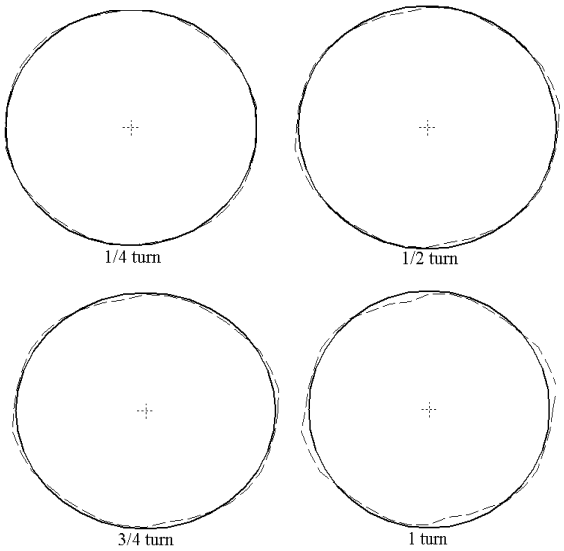

Fig. 6. Distortion of the stator inner perimeter

2.2 Experimental Results

We conducted some experiments on mechanical vibration using an accelerometer. As shown in Fig. 7, an accelerometer, SENSOTEC-SM5 (0-600 Hz

BW), was installed at the 90° position above the shaft. The motor under test was a 3-phase induction motor, 1 hp, 380V, 50 Hz. The supply was clean and balanced. Fig. 8 and Fig. 9 depict the time-domain results, and the spectrum of the displacements, respectively. It is noticed that our simulated results agree with the measured ones in terms of phase, and frequencies. However, there are some magnitude differences because our simulations did not take account of the effects of clearance, damping, thermal expansion, and motor eccentricity.

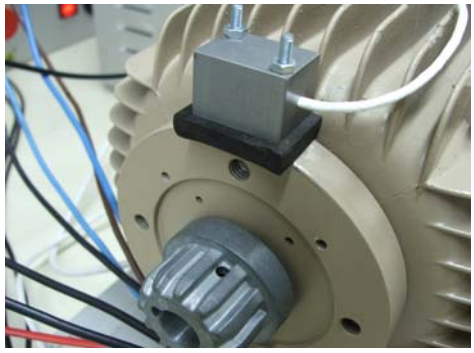

Fig. 7. Position of the accelerometer for test

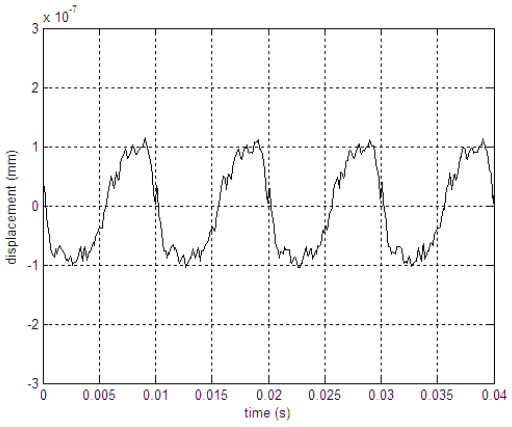

Fig. 8. Displacement: a) simulated, b) measured

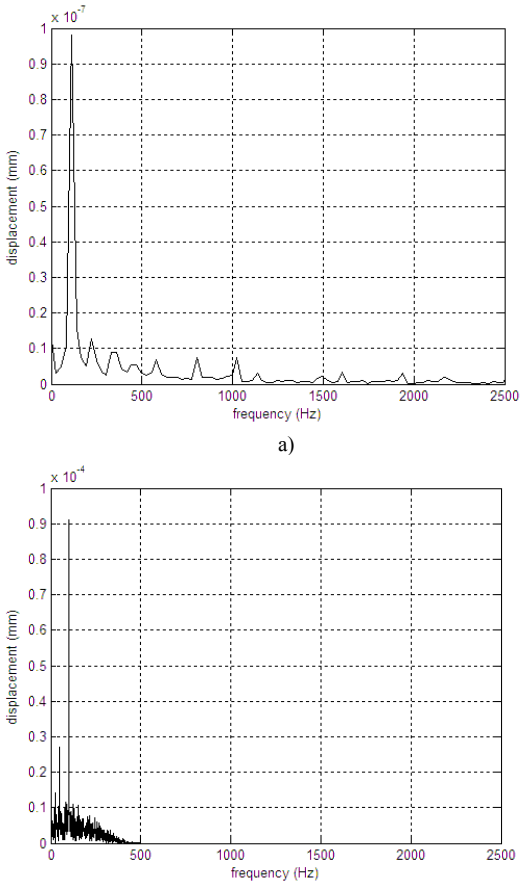

Fig. 9. Spectrum of displacement: a) simulated, b) measured

3 Effects of Nonsinusoidal Voltages on Current Harmonics

We consider three different voltage sources applied to the motor, i.e. a sinusoidal source, a PWM VSI, and a six-step VSI, respectively. The waveforms of the applied voltages and the motor stator currents are shown in Fig. 10. The sources introduce different shapes of the stator currents having their rms values of 9.02 A, 9.16 A and 10.02 A, respectively. The ideal sinusoidal source produces stator current with the least harmonic.

The curl of the magnetic vector potential **A** is magnetic flux density **B** (**B** = ∇×**A**). The Maxwell's stress equations were used to determine the distribution of the magnetic forces across the air gap. The surface plots in Fig. 11(a) – 11(c) disclose the space-time distributions of the radial forces according to the round trapezoidal slot when the motor is excited by an ideal source, a PWM VSI, and a six-step VSI, respectively. For the rectangular and round slots, similar results are obtained with different magnitudes. Calculation of the total

harmonic distortion (THD) is conducted for each stator tooth (36 altogether), then the average, THD_{avg}, is calculated. Corresponding to each type of sources, the following THD_{avg} values (in %) are obtained: 43.27, 70.29, and 78.08, respectively. With realistic drive technology, PWM drive produces less harmonic contents than six-step VSI does. The shapes of voltage and current excitations obviously influence the shapes of these distributions. In other words, the harmonic contents in the motor's excitations affect the smoothness of the distributions, and can be used for motor vibration analysis.

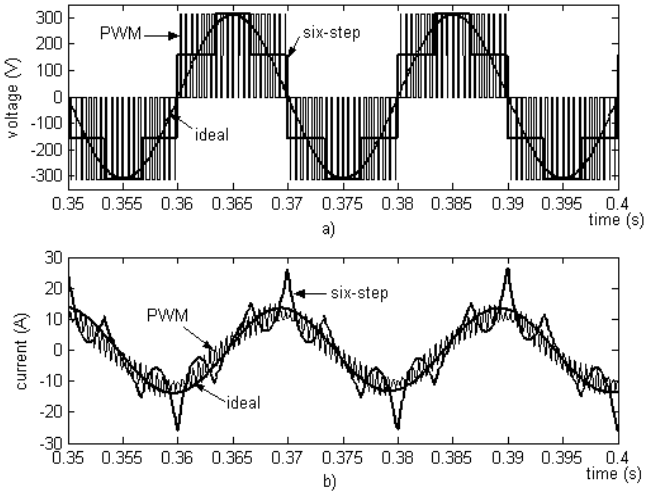

Fig. 10. Steady-state waveforms: a) applied stator voltages, b) applied stator currents

4 Effects of Rotor-Slot Geometry on Mechanical Vibrations

The motor is assumed to have sinusoidal excitation, and three different shapes of rotor slots for comparison purposes as shown in Fig. 1. The FEM solver provides solutions disclosing the distortion of the stator inner perimeter as shown in Fig. 12. The average displacements in one revolution are 6.0924×10^{-8}, 6.1963×10^{-8}, and 5.8989×10^{-8} mm corresponding to the round trapezoidal slot, the rectangular slot and the round slot, respectively. Hence, the round slot renders the least lateral vibration, and the rectangular slot is not a good candidate. It is observed that the depth and the geometry of the slots affect the amount of vibration. A deeper slot results in more flux leakage, and hence more vibration.

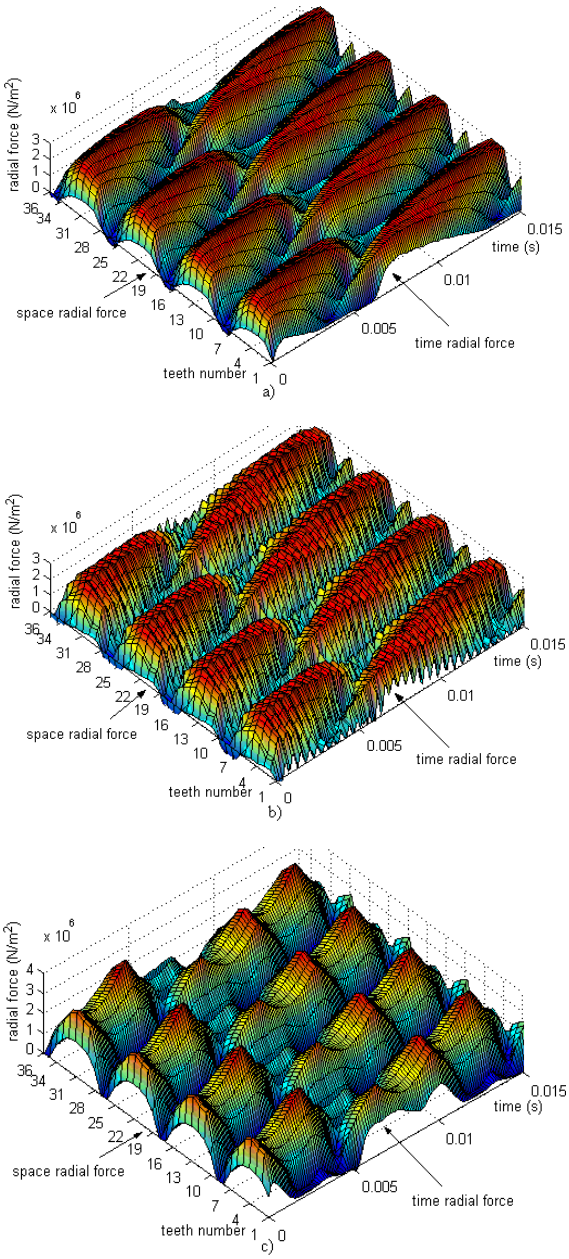

Fig. 11. Space-time distribution of radial forces according to three different sources: a) sinusoidal source, b) PWM VSI, c) six-step VSI

5 Conclusions

This paper presents the mathematical models, the graphical results, and the interpretation for the motor vibration resulting from the induced electromagnetic forces. By using the N-R method embedded with the BCG method, the nonlinearity of magnetic core saturation can be solved numerically. The simulation results show good agreement with the measurement results. To demonstrate the usefulness of our approach, the three IEEE standard rotor slot shapes of equal slot areas are chosen for competition. In addition, three different voltage sources (pure

sinusoid, PWM VSI, and six-step VSI) are used to excite the motor correspondingly. As a result, the motors with purely sinusoidal excitation are subjected to the minimum vibration, whilst the maximum vibration occurs with the six-step inverter supply, of which voltage and current waveforms contain a great deal of harmonics. It can be concluded that an important factor contributing to the motor vibration is current harmonics. The motor vibration is also affected by the geometrical shape of the rotor slots. Deeper slots are expected to produce more vibration. However, for completion of rotor design, other factors, such as torque-speed curves, etc., are also vital and should be considered during the design phase. The slot geometry must be optimized to ensure the motor class with minimum vibration. Our approach is suitable for the task.

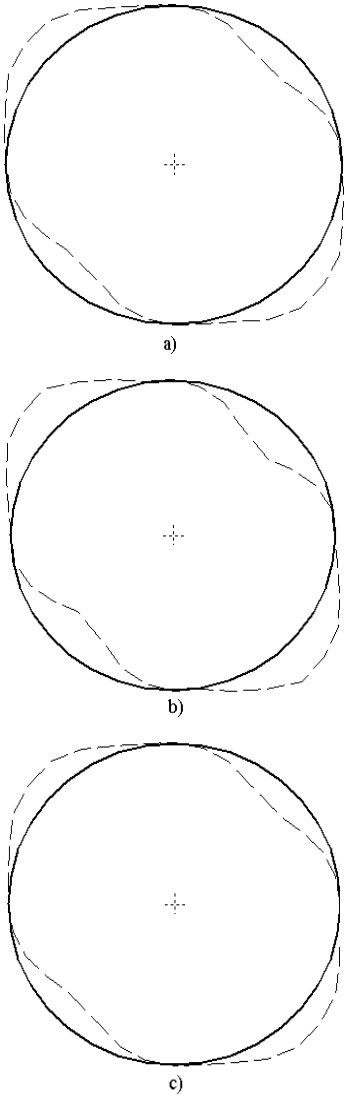

Fig. 12. Instantaneous distortion of the stator inner perimeters: a) round trapezoidal slot, b) rectangular slot, c) round slot

References:

[1] R.J.M. Belmans, D. Verdyck, W. Geysen, and R.D. Findlay, Electro-mechanical analysis of the audible noise of an inverter-fed squirrel-cage induction motor, *IEEE Transactions on Industry Applications,* Vol.27, No.3, 1991, pp. 539-544.

[2] W.R. Finley, Noise in induction motors-causes and treatments, *IEEE Transactions on Industry Applications,* Vol.27, No.6, 1991, pp. 1204-1213.

[3] D.G. Dorrell, Calculation of unbalanced magnetic pull in small cage induction motors with skewed rotors and dynamic rotor eccentricity, *IEEE Transactions on Energy Conversion,* Vol.11, No.3, 1996, pp. 483-488.

[4] D.H. Im, J.H. Chang, S.C. Park, B.I. Kwon, J.P. Hong, and B.T. Kim, Analysis of radial force as a source of vibration in an induction motor with skewed slots, *IEEE Transactions on Magnetics*, Vol.33, No.2, 1997, pp. 1650-1653.

[5] T. Kobayashi, F. Tajima, M. Ito, and S. Shibukawa, Effects of slot combination on acoustic noise from induction motors, *IEEE Transactions on Magnetics,* Vol.33, No.2, 1997, pp. 2101-2104.

[6] B.T. Kim, B.I. Kwon, and S.C.Park, Reduction of electromagnetic force harmonics in asynchronous traction motor by adapting the rotor slot number, *IEEE Transactions on Magnetics,* Vol.35, No.5, 1999, pp. 3742-3744.

[7] I. Boldea, and S.A. Naser, *The induction machine handbook*, Florida, USA, 2002.

[8] S.J. Yang, *Low-Noise Electrical Motors,* Oxford University Press, New York, 1981.

[9] W.H. Hayt, *Engineering Electromagnetic,*5th ed., McGraw-Hill, Singapore, 1989.

[10] W.N. Fu, *Electromagnetic field analysis of induction motors by finite element method and its application to phantom loading,* Ph.D. Thesis, Hong Kong Polytechnic University, China, 1999.

[11] E. Vassent, G. Meunier, and A. Foggia, Simulation of induction machines-using complex magnetodynamic finite element method coupled with the circuit equations*, IEEE Transactions on Magnetics*, Vol.27, No.5, 1991, pp. 4246-4249.

[12] M.E. Nagwa, R.E. Anthony, and E.D. Graham, Detection of broken bars in the cage rotor on an induction machine, *IEEE Transactions on Industry Applications,* Vol.28, No.1, 1992, pp. 165-171.

[13] K. Umashankar and A. Taflove, *Computational Electromagnetics.* Artech House, London, 1993.

[14] T.W. Preston, A.B.J. Reece, and P.S. Sangha, Induction motor analysis by time-stepping techniques, *IEEE Transactions on Magnetics*, Vol.24, No.1, 1988, pp. 471-474.

[15] M.A. Jabbar, N.P. Hla, L. Zhejie, and B. Chao, Modeling and numerical simulation of a brushless permanent-magnet dc motor in dynamic conditions by time-stepping technique, *IEEE Transactions on Industry Applications*, Vol. 40, No.3, 2004, pp. 763-770.

[16] W.H. Press, S.A. Teukolsky, W.T. Vetterling, and B.P. Flannery, *Numerical Recipes in C,* 2nd ed., Cambridge University press, USA, 1999.

[17] F. Ishibashi, K. Kamimoto, S. Noda, and K. Itomi, Small induction motor noise calculation, *IEEE Transactions on Energy Conversion,* Vol.18, No.3, 2003, pp. 357-361.

[18] J.S. Rao, *Dynamics of plates*, Narosa Publisher, New Delhi, 1999.